PERGAMON

Journal of the Mechanics and Physics of Solids
51 (2003) 147–167

JOURNAL OF THE
MECHANICS AND
PHYSICS OF SOLIDS

www.elsevier.com/locate/jmps

The orientation of the self-assembled monolayer stripes on a crystalline substrate

Y.F. Gao*, Z. Suo

Mechanical and Aerospace Engineering Department and Princeton Materials Institute, Princeton University, Princeton, NJ 08544, USA

Received 18 January 2002; accepted 21 June 2002

Abstract

Two-phase monolayers adsorbed on crystalline substrates can form many patterns. After reviewing the experimentally observed patterns on various substrates, we extend a thermodynamic theory to account for the anisotropy in surface stress, substrate stiffness, and phase boundary energy. We solve the elastic field in the anisotropic substrate by using the Stroh formalism. We then focus on the pattern of periodic stripes, and determine the orientation of the stripes that minimizes the free energy. As an example, we examine in detail the (1 1 0) surface of a cubic crystal. Depending on the parameters that characterize anisotropy, the stripes can orient along either $[\bar{1}\,1\,0]$, or [0 0 1], or certain directions off the two crystalline axes. The transition between these orientations can be of either first or second order. The predications point to additional experiments that are needed to further the understanding.

Keywords: Self-assembly; Nanostructure; Monolayer; Anisotropy; Surface stress

1. Introduction

In recent decades, the invention of new instruments, such as the scanning tunneling microscope, has led to a burst of research activities in investigating the solid surfaces at atomic or molecular level. Experiments have shown that adsorbed monolayers, when separating into distinct phases, can self-assemble into various two-dimensional patterns, including periodic stripes, triangular lattices, square lattices, and irregular arrangements (Kern et al., 1991; Leibsle et al., 1993; Zeppenfeld et al., 1994, 1995; Pohl et al., 1999; Ellmer et al., 2001; Plass et al., 2001). The feature size of the patterns is on the order

* Corresponding author. Tel.: +1-609-258-5777; fax: +1-609-258-5877.
E-mail address: ygao@princeton.edu (Y.F. Gao).

0022-5096/02/$ - see front matter
PII: S0022-5096(02)00053-4

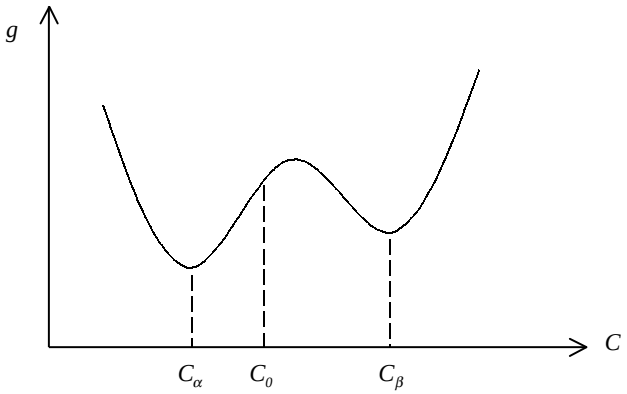

Fig. 1. The free energy of mixing has two wells, corresponding to two phases.

1–100 nm, and is often stable on annealing. The self-assembled patterns have potential applications, e.g., as templates to grow functional nanostructures (Li et al., 1999).

The patterns form to minimize the combined free energy of mixing, phase boundary, and elastic field (Alerhand et al., 1988; Ng and Vanderbilt, 1995; Zeppenfeld et al., 1995; Suo and Lu, 2000). On the solid surface, the monolayer consists of two atomic species. For the two-dimensional mixture, Fig. 1 shows the free energy of mixing g as a function of the concentration C (i.e., the fraction of surface sites covered by one of the two atomic species). The function $g(C)$ has two wells at concentrations C_α and C_β, corresponding to two phases α and β. If the average concentration of the monolayer, C_0, is between C_α and C_β, to lower the integrated free energy of mixing, the monolayer separates into the two phases. The boundaries between the two phases are lines with excess energy, and drive the two phases to *coarsen*. The surface stresses in the two phases are different, causing an elastic field in the substrate. The smaller the size of the phases, the better the substrate deformation accommodates the difference in the surface stress. Consequently, the surface stress difference drives the two phases to *refine*. The competition between the phase boundary energy and the elastic energy selects an equilibrium phase size. We consider the annealing process, in which the deposition process has stopped, but atoms can relocate within the surface by diffusion, effecting the morphological change of the phases.

A powerful way to obtain diverse patterns is to use substrate with various crystalline symmetries. Although experiments have been done on substrates of several materials and crystalline orientations, theories so far have mainly been for the isotropic substrate. This paper, together with our recent work (Lu and Suo, 2002a,b; Gao et al., 2002), aims to fill this gap. First we summarize the available experiments and theories, grouping them according to the crystalline symmetry of the substrate. Then we extend a thermodynamic theory to account for anisotropy in phase boundary energy, surface stress, and substrate stiffness. We solve the anisotropic elasticity boundary value problem by using the Stroh (1958) representation in the appendix. The solution method is quite general, and is likely to find applications to other phenomena.

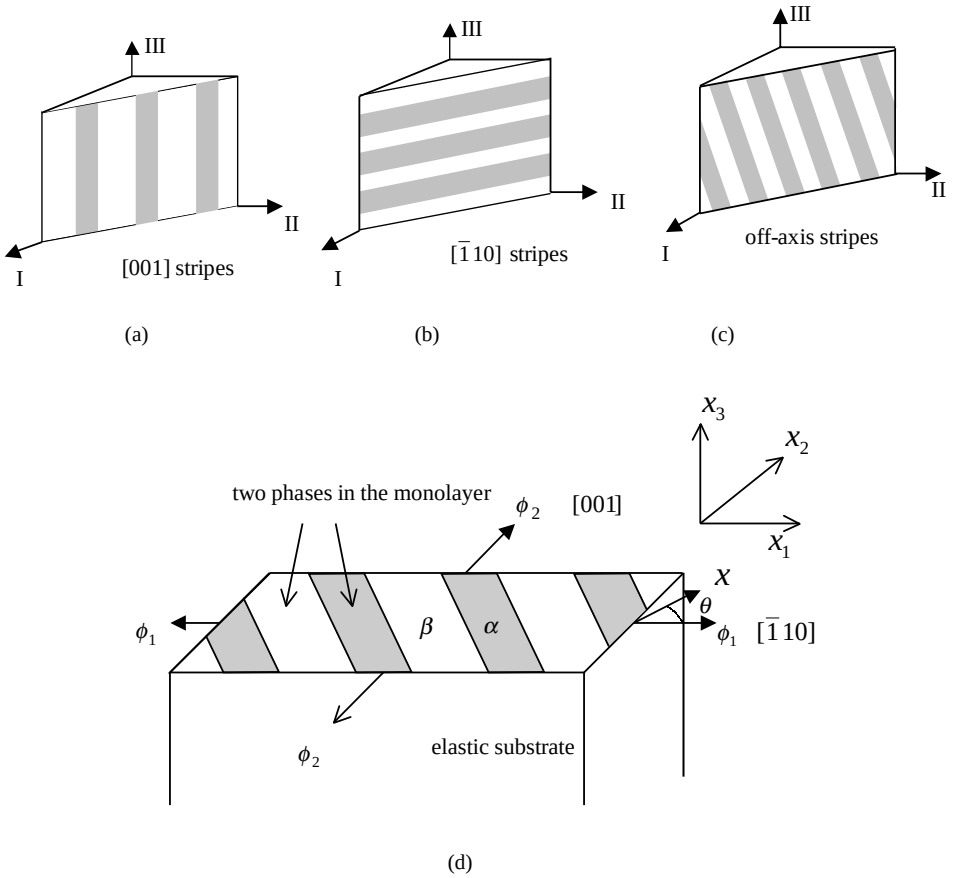

Fig. 2. (a) The [0 0 1] stripes in the coordinates formed by the principal crystalline axes; (b) the [$\bar{1}$ 1 0] stripes; (c) the off-axis stripes (i.e., the θ stripes); (d) the coordinates used in the calculations.

To illustrate the theory, we study periodic stripes formed on the (1 1 0) surface of a cubic crystal. The (1 1 0) surface has fewer symmetry operations compared to other commonly used substrates, such as the (1 0 0) or (1 1 1) surface of a cubic crystal, or the (0 0 0 1) surface of a hexagonal crystals. Consequently, patterns on the (1 1 0) surface are relatively easier to interpret. The equilibrium concentration field is a state that minimizes the free energy. Our calculation shows that, depending on the parameters that characterize anisotropy, the stripes can orient along either [$\bar{1}$ 1 0], or [0 0 1], or certain directions off the two crystalline axes. Figs. 2a–c show the three cases. The case illustrated in Fig. 2c is quite remarkable, given the two-fold symmetry on the (1 1 0) substrate.

Fig. 2d shows the coordinates to be used. The substrate is semi-infinite, occupying the half space $x_3 < 0$. The monolayer coincides with the plane (x_1, x_2), the [$\bar{1}$ 1 0] axis with x_1, and the [0 0 1] axis with x_2. The orientation angle, θ, is measured from the

$[\bar{1}\,1\,0]$ axis to the direction x in which the concentration varies. We determine the equilibrium stripe orientation as a function of the parameters representing anisotropy.

In this paper, we ignore the surface steps on the clean metal surfaces. Few studies have been made on the effect of those steps on the observed patterns. In the experiment of Kern et al. (1991), the oxygen stripes were observed to go through the steps without changing orientation and shape.

2. Symmetry breaking in monolayer patterns: existing experiments and theories

To motivate this work, we briefly review existing experiments according to crystalline symmetry of the substrate. Kern et al. (1991) studied oxygen on Cu (1 1 0) surface. On annealing, oxygen atoms arranged into stripes that alternate with bare copper stripes, running along the [0 0 1] direction. The width of the individual oxygen stripe, depending on oxygen coverage and temperature, varies between 6 and 14 nm. It is believed that the low symmetry substrate surface guides the orientation of the oxygen stripes. We will see later in this paper the conditions under which the [0 0 1] stripes prevail over the $[\bar{1}\,1\,0]$ stripes.

Zeppenfeld et al. (1995) investigated Ag on Pt(1 1 1) surface. At a low coverage, Ag atoms form islands with a short-range order. At a high coverage, Ag atoms form meandering stripes. Pohl et al. (1999) deposited a monolayer of Ag on a Ru (0 0 0 1) surface, and then exposed the Ag-covered Ru to sulfur. The epilayer became a two-dimensional composite of sulfur disks in a Ag matrix. The sulfur disks were of diameter about 3.4 nm, and formed a triangular lattice. Plass et al. (2001) studied Pb on Cu(1 1 1) surface. The surface mixture separates into two phases: a Pb–Cu surface alloy (α), and a Pb overlayer (β). Upon increasing the Pb coverage, these authors observed a sequence of domain patterns, namely, islands of β in the background of α, alternating stripes of α and β, and islands of α in the background of β. The above three experiments on the surfaces with three-fold symmetry demonstrated the formation of triangular lattices, and the transition from the lattices to stripes. Due to symmetry, the stripes did not line up in a single direction.

Leibsle et al. (1993) and Ellmer et al. (2001) studied nitrogen on Cu(1 0 0) surface. After annealing, the surface was covered by a regular square lattice of nitrogen islands, approximately 5 nm across, with the sides parallel to the [0 0 1] direction. In addition, Ellmer et al. (2001) found at low and high nitrogen coverage two-dimensional array of compact nitrogen islands formed, while a quasi-1D arrangement of striped pattern (rows of squares) was in the intermediate coverage. A small amount of gold, pre-deposited on the bare copper surface, changed the orientation of the square lattices to [1 1 0] direction.

We have modeled symmetry breaking in two-phase monolayers in several previous papers (Lu and Suo, 2001, Lu and Suo, 2002a,b; Gao et al., 2002). When the system was isotropic, depending on the average concentration, the two-phase mixture formed either polygrained triangular lattices or meandering stripes. The symmetry was broken when some anisotropy was introduced. Periodic stripes along certain directions or herringbone structures were formed. So far the theory has been limited to two

special cases: (0 0 1) surface of a cubic crystal with isotropic surface stress and isotropic phase boundary energy (Lu and Suo, 2002b), and an elastically isotropic substrate with anisotropic surface stress and isotropic phase boundary energy (Lu and Suo, 2002a; Gao et al., 2002). This paper further extends this sequence of work to account for all modes of anisotropy: surface stress, phase boundary energy, and substrate stiffness. The extended theory can treat any crystal plane and any elastic anisotropy.

3. The thermodynamic theory of pattern formation

Following Suo and Lu (2000), we construct a thermodynamic theory of the substrate-monolayer system by prescribing a procedure to calculate its free energy. The free energy of the monolayer-substrate system consists of two parts: the bulk elastic energy, and the excess surface energy. Write

$$G = \int W \, \mathrm{d}V + \int \Gamma \, \mathrm{d}A. \tag{1}$$

Here W is the elastic energy per unit volume, and is integrated over the volume of the substrate. Γ is the excess surface energy per unit area, and is integrated over the surface area covered by the monolayer. Both V and A are measured in the undeformed configuration of the substrate.

Assume that the deformation in the substrate is infinitesimal, so that the strain tensor, ε_{ij}, relates to the displacement vector, u_i, as

$$\varepsilon_{ij} = \tfrac{1}{2}(u_{i,j} + u_{j,i}). \tag{2}$$

A Latin subscript runs from 1 to 3. The substrate is linearly elastic and generally anisotropic, relating the stress tensor and the strain tensor as

$$\sigma_{ij} = c_{ijkl}\varepsilon_{kl}. \tag{3}$$

The repeated subscripts imply the summation convention. The stiffness tensor, c_{ijkl}, obeys the usual relations:

$$c_{ijkl} = c_{klij} = c_{jikl} = c_{ijlk}. \tag{4}$$

The stiffness tensor is known once the material and the orientation of the substrate are specified. The elastic energy density is quadratic in the strain, namely,

$$W = \tfrac{1}{2}\, c_{ijkl}\varepsilon_{ij}\varepsilon_{kl}. \tag{5}$$

To represent the effects of the free energy of mixing, the phase boundary energy, and the surface stress, we take the following approach. Assume that the surface energy density Γ is a function of the concentration C, the concentration gradient $C_{,\alpha}$, and the strain in the surface, $\varepsilon_{\alpha\beta}$. Greek subscripts run from 1 to 2. Expand the surface energy density to the leading order power series in the concentration gradient and the strain, and we have

$$\Gamma = g + hC_{,\beta}C_{,\beta} + f_{\alpha\beta}\varepsilon_{\alpha\beta}. \tag{6}$$

The leading term in the concentration gradient is quadratic, because the symmetry excludes the term linear in the concentration gradient.

When the concentration field is uniform, the surface stress is also uniform, so that the semi-infinite substrate is unstrained, and only g remains in Eq. (6). Consequently, g represents the free energy of mixing, and is a function of the concentration. In order for the surface mixture to separate into two phases, we assume that the function $g(C)$ has two wells as shown in Fig. 1. We assume that the function $g(C)$ is known, but its detailed form is unimportant to this work.

In Eq. (6), following Cahn and Hilliard (1958), we represent the phase boundary energy by the term quadratic in the concentration gradient. The coefficient h is generally a function of the concentration and the direction of the concentration gradient. In principle, the phase boundary energy can be calculated from an atomistic model, but we are unaware of any such calculations for the two-phase monolayers. In this paper, we will simply treat the function h phenomenologically. Since we will study periodic stripes on the (1 1 0) surface of a cubic crystal, we assume that h is a function of stripe orientation θ as

$$h(\theta) = h_0 H(\theta), \quad H(\theta) = 1 + \gamma \cos 2\theta. \tag{7}$$

The positive constant, h_0, scales the magnitude of the phase boundary energy. The function $H(\theta)$ has two-fold symmetry; any other function of two-fold symmetry will serve the purpose. The parameter γ measures the anisotropy in the phase boundary energy. When $\gamma = 0$, the phase boundary energy is isotropic. When $\gamma > 0, h$ minimizes at $\theta = \pi/2, 3\pi/2$, and the phase boundary energy anisotropy favors the $[\bar{1}\,1\,0]$ stripes (Fig. 2b). When $\gamma < 0$, h minimizes at $\theta = 0, \pi$, and the phase boundary energy anisotropy favors the [0 0 1] stripes (Fig. 2a).

Expansion (6) has neglected terms quadratic in strains; this is equivalent to saying that the monolayer has a similar elastic modulus as the substrate, so that the bulk strains give no excess surface elastic energy.

We assume that the surface stress tensor $f_{\alpha\beta}$ is linear in the concentration C. That is, when the concentration changes by ΔC, the surface stress changes by

$$\Delta f_{\alpha\beta} = \phi_{\alpha\beta} \Delta C. \tag{8}$$

The slope tensor $\phi_{\alpha\beta}$ depends on the materials system, and can be measured by the wafer curvature method (Ibach, 1997). As illustrated in Fig. 2d, the principal components of the slope tensor, ϕ_1 and ϕ_2, are taken to be in the directions x_1 and x_2. Let

$$\phi_1 = \phi \cos \omega, \quad \phi_2 = \phi \sin \omega, \tag{9}$$

where $\phi = \sqrt{\phi_1^2 + \phi_2^2}$ measures the magnitude of the slope tensor, and ω measures its anisotropy. Fig. 3 illustrates both the rectangular coordinates (ϕ_1, ϕ_2) and the polar coordinates (ϕ, ω).

Given a displacement field in the substrate, $u_i(x_1, x_2, x_3)$, and the concentration field in the monolayer, $C(x_1, x_2)$, the above procedure calculates the free energy of the substrate-monolayer system. That is, we have prescribed a thermodynamic theory of the system. We next study the most important property of this theory: the equilibrium states. The system varies its free energy by two means: the elastic deformation in the substrate, and atomic diffusion in the monolayer. The system strives to attain both

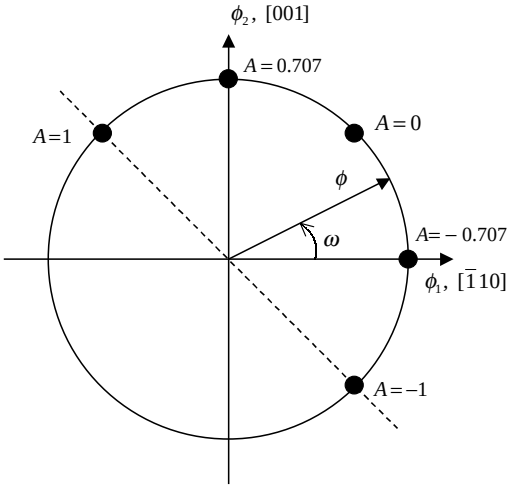

Fig. 3. The coordinate plane that represents surface stress anisotropy. The parameter A is defined as $A = (\phi_2 - \phi_1)/\sqrt{2}\phi$.

elastic and diffusive equilibria. A trivial equilibrium state exists: the concentration field is uniform in the monolayer, and the displacement vanishes in the substrate. Under certain conditions, however, this trivial equilibrium state is unstable. That is, the free energy is minimized by certain nonuniform states, leading to concentration patterns. We study these nonuniform equilibrium states.

The system attains elastic equilibrium when the free energy variation associated with the variation in the elastic displacement vanishes. The functional calculus gives the field equation inside the substrate:

$$\sigma_{ij,j} = 0 \tag{10}$$

and the traction vector on the surface of the substrate

$$\sigma_{31} = \phi_1 \frac{\partial C}{\partial x_1}, \quad \sigma_{32} = \phi_2 \frac{\partial C}{\partial x_2}, \quad \sigma_{33} = 0. \tag{11}$$

Consequently, for a given concentration field, elastic equilibrium defines an elasticity boundary value problem in the anisotropic semi-infinite solid with prescribed surface traction. The appendix solves this elasticity boundary value problem by using the Stroh (1958) formalism. Note that the trivial equilibrium state described above indeed satisfies all the equations.

Because the elasticity boundary value problem is a linear one, the stress, the strain, and the displacement fields are all linear in the slope tensor, $\phi_{\alpha\beta}$. Furthermore, because the traction boundary conditions (11) are prescribed, the strain and the displacement fields are linear in the compliance tensor (i.e., the inverse of the stiffness tensor). Consequently, the elastic energy stored in the substrate is quadratic in the slope tensor $\phi_{\alpha\beta}$, and is linear in the compliance tensor.

The elastic equilibrium conditions, in conjunction with the divergence theorem, reduce the free energy (1) to

$$G = \int \left(g + hC_{,\alpha}C_{,\alpha} - \frac{1}{2}\sigma_{3\alpha}u_{\alpha} \right) \mathrm{d}A. \tag{12}$$

The integral extends over the entire substrate surface. Note that $\int \frac{1}{2}\sigma_{3\alpha}u_{\alpha}\,\mathrm{d}A$ is the elastic energy stored in the volume of the substrate. One can confirm that the surface stress term in Eq. (6), $\int f_{\alpha\beta}\varepsilon_{\alpha\beta}\,\mathrm{d}A$, is negative and is twice the elastic energy stored in the substrate. Consequently, the sum of the two terms gives what appears in Eq. (12), with the negative sign. Remarkably, the more the elastic energy in the substrate, the lower the free energy of the monolayer-substrate system.

For any given concentration field $C(x_1, x_2)$, after the equilibrium elastic field in the substrate is solved, Eq. (12) gives the free energy in the substrate-monolayer system. If the concentration is uniform, being C_0 everywhere in the monolayer, the second and the third terms in Eq. (12) vanish. If $C_\alpha < C_0 < C_\beta$, as shown in Fig. 1, the free energy of mixing reduces once the uniform monolayer separates into the two phases, α and β. The nonuniform concentration field adds the phase boundary energy to the system, represented by the second term in Eq. (12). The nonuniform concentration field adds elastic energy to the substrate, but reduces the surface energy through the action of the surface stress, the net effect being represented by the third term in Eq. (12), which lowers the free energy of the substrate-monolayer system. The diffusive equilibrium is attained by minimizing the free energy (12) by varying the concentration field.

4. Periodic stripes: the equilibrium period and orientation

We now calculate the free energy of the monolayer-substrate system, assuming that the concentration field forms periodic stripes. The concentration is now nonuniform, varying in the direction x (Fig. 2d). Represent the concentration field by a Fourier series in the x coordinate,

$$C(x) = \sum_{n=-\infty}^{+\infty} C_n \exp(\mathrm{i}n\alpha), \qquad \alpha = 2\pi x/\lambda, \tag{13}$$

where λ is the period of the concentration field. To ensure that C is real-valued, we require that $C_{(-n)} = \bar{C}_n$, where a bar on the top of a quantity denotes the complex conjugate. Because no atoms leave or enter the monolayer during annealing, the average concentration, C_0, remains constant. The period λ, the Fourier coefficients C_n ($n \neq 0$), and the orientation θ are varied to minimize the free energy.

The free energy per unit area is calculated by the free energy in a period divided by the period, namely,

$$\tilde{G} = \frac{1}{2\pi}\int_0^{2\pi} G\,\mathrm{d}\alpha. \tag{14}$$

The calculation gives

$$\tilde{G} = \tilde{g} + \frac{1}{2}Sh_0H\left(\frac{2\pi}{\lambda}\right)^2 - \frac{\phi^2}{4c_{1111}}Q\Theta\left(\frac{2\pi}{\lambda}\right), \tag{15}$$

where

$$\tilde{g} = \frac{1}{2\pi}\int_0^{2\pi} g(C)\,\mathrm{d}\alpha, \tag{16}$$

$$S = 2\sum_{n=-\infty}^{+\infty} n^2|C_n|^2, \tag{17}$$

$$Q = 2\sum_{n=-\infty}^{+\infty} n|C_n|^2, \tag{18}$$

$$\Theta = \mathbf{m}^{\mathrm{T}} M \mathbf{m}, \tag{19}$$

$$\mathbf{m} = (\cos\theta\cos\omega,\ \sin\theta\sin\omega,\ 0)^{\mathrm{T}}. \tag{20}$$

Only the calculation of the elastic energy is nontrivial, which is carried out in the appendix. As defined in the appendix, the matrix M is symmetric and positive-definite. Consequently, the elastic interaction lowers the free energy, as expected. The matrix M is dimensionless, and depends on the ratios of the components of the stiffness tensor.

A comparison of the phase boundary energy and the elastic energy in Eq. (15) determines a length scale

$$l = \frac{c_{1111}h_0}{\phi^2}. \tag{21}$$

The magnitude of stiffness is $c_{1111} \sim 10^{11}$ N/m^2. The magnitude of h_0 is of the order of energy per atom at the phase boundary, $h_0 \sim 10^{-19}$ J . According to Ibach (1997), the magnitude of the surface stress slope tensor is about $\phi \sim 3$ N/m. With these estimates, we find that $l \sim 1$ nm.

Examine the free energy (15) as a function of the period λ. The term $\tilde{g}$ is the average free energy of mixing, and is independent of λ. The second term in Eq. (15) comes from the phase boundary energy, and decreases when the period λ increases, so that the term drives phase coarsening. The third term in Eq. (15) comes from the surface stress and the substrate elasticity, and decreases when the period λ decreases, so that the term drives phase refining. $\tilde{G}$ is quadratic in $(2\pi/\lambda)$, and reaches the minimum when the period is

$$\lambda_{\mathrm{eq}} = \frac{8\pi SH}{Q\Theta}\,l. \tag{22}$$

The equilibrium period scales with l, which in turn is set by the competition between the phase boundary energy and the surface stress.

If the system is isotropic, $\phi^2 = 2\phi_1^2$, $c_{1111} = 2(1-\nu)/(1-2\nu)\mu$, $H = 1$ and $\Theta = (1-\nu)^2/(1-2\nu)$, where ν is Poisson's ratio, and μ is the shear modulus. Furthermore, if only the terms $n = -1, 0, 1$ are retained in the Fourier series (13), $S = Q$. Under these conditions, $\lambda_{\mathrm{eq}} = 16\pi\mu h_0/(1-\nu)\phi^2$. This recovers the result which was first obtained in a linear perturbation analysis (Lu and Suo, 1999), and serves as a rough estimate of the equilibrium period. (The definition in Eq. (21) differs from that in our previous work by the factor $\Theta/2$.)

Combining Eqs. (15) and (22), we write the average free energy in the form

$$\tilde{G} = \tilde{g} + g_1 \Psi, \tag{23}$$

where

$$g_1 = \frac{\phi^2 Q^2}{32 c_{1111} l S}, \tag{24}$$

$$\Psi = -\frac{\Theta^2}{H}. \tag{25}$$

An inspection shows that both $\tilde{g}$ and g_1 are independent of θ. Consequently, to determine the equilibrium orientation, we only need to minimize Ψ as a function of θ. Once the equilibrium orientation is determined, the Fourier coefficients C_n can be determined by minimizing $\tilde{G}$. The procedure is the same as that in Gao et al. (2002).

In this paper, we will focus on the equilibrium orientation of the stripes. To evaluate $\Psi(\theta)$, we need first to calculate the matrix M defined in the appendix, and then to obtain Θ by using Eqs. (19) and (20). Compared with the numerical integration of a diffusion equation, which was heavily used in our previous work, the amount of computation here is insignificant.

5. The (1 1 0) surface of a cubic crystal

For a cubic crystal, the stiffness tensor has three independent components, i.e., c_{11}, c_{12}, c_{44} in the abbreviated notation. The requirement that the elastic energy be positive for any arbitrary strain tensor places the following restrictions on the three elastic moduli:

$$c_{11} > 0, \quad c_{44} > 0, \quad -0.5 < c_{12}/c_{11} < 1. \tag{26}$$

Define two dimensionless parameters

$$\eta = c_{12}/c_{11}, \quad \zeta = \frac{c_{12} + 2c_{44}}{c_{11}} - 1, \tag{27}$$

which have restrictions: $-0.5 < \eta < 1$, and $\eta - 1 < \zeta < +\infty$. The parameter ζ measures the stiffness anisotropy of a cubic crystal. When $\zeta = 0$, the crystal is elastically isotropic. For Cu, $\eta = 0.721$ and $\zeta = 0.6164$; for Mo, $\eta = 0.3826$ and $\zeta = -0.1391$. A tensor transformation gives the stiffness components c_{ijkl} in the coordinate system specified in Fig. 2d.

The effect of substrate stiffness is understood qualitatively as follows. Recall that the strain and displacement fields are linear in the compliance tensor. Everything else being equal, the more compliant the substrate is, the better it can accommodate the surface stress difference in the two phases. Because of the anisotropy in the stiffness tensor, stripes in different orientations can induce different amount elastic energy in the substrate. Consequently, it is worthwhile to examine stiffness components in various orientations.

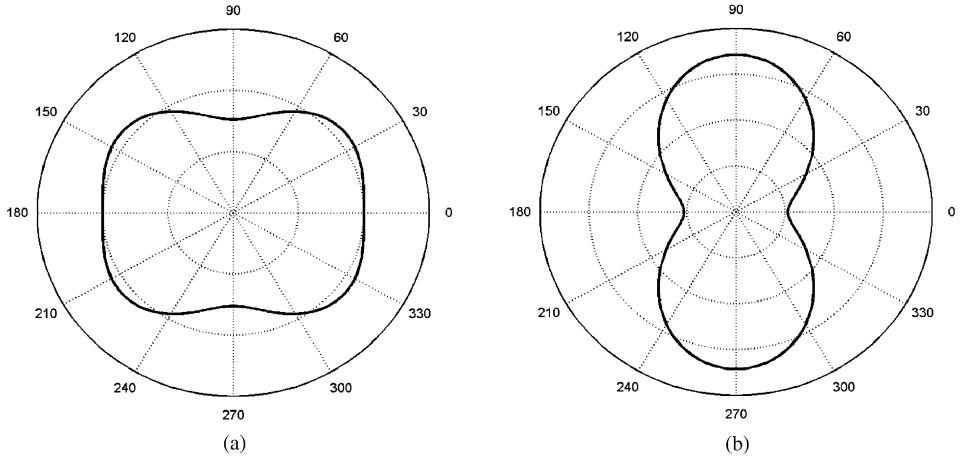

Fig. 4. The stiffness versus orientation for Cu in polar coordinates: (a) The tensile stiffness in the x direction; (b) the shear stiffness in the plane (x, x_3).

Let $\mathbf{p}$ be a unit vector. The tensile stiffness in the direction $\mathbf{p}$ is

$$c_t = c_{ijkl}\, p_i\, p_j\, p_k\, p_l. \tag{28}$$

For a cubic crystal, let p_i be the vector components along the crystalline axes. The tensile stiffness is

$$\frac{c_t}{c_{11}} = 1 + \zeta(1 - p_1^4 - p_2^4 - p_3^4). \tag{29}$$

When $\mathbf{p}$ coincides with the x direction in Fig. 2d, $\mathbf{p} = (-\cos\theta/\sqrt{2}, \cos\theta/\sqrt{2}, \sin\theta)^{\mathrm{T}}$, so that

$$\frac{c_t}{c_{11}} = 1 + \zeta\left(1 - \frac{1}{2}\cos^4\theta - \sin^4\theta\right). \tag{30}$$

Fig. 4a plots function (30) in the polar coordinates, using the parameter ζ for Cu. The tensile stiffness minimizes at $\theta = \pi/2$ and $3\pi/2$. Consequently, the tensile modulus anisotropy favors the $[\bar{1}\,1\,0]$ stripes. Obviously, the tensile stiffness in the x_3 direction is independent of θ, and is therefore not discussed here.

Next examine the shear modulus. Let $\mathbf{p}$ and $\mathbf{q}$ be two perpendicular unit vectors. The shear modulus in the directions $\mathbf{p}$ and $\mathbf{q}$ is

$$c_s = c_{ijkl}\, p_i q_j\, p_k q_l. \tag{31}$$

For a cubic crystal, this reduces to

$$\frac{c_s}{c_{11}} = \frac{c_{44}}{c_{11}} - \zeta(p_1^2 q_1^2 + p_2^2 q_2^2 + p_3^2 q_3^2). \tag{32}$$

In Fig. 2d, when $\mathbf{p}$ coincides with the x direction, and $\mathbf{q}$ with x_3, we have $\mathbf{p} = (-\cos\theta/\sqrt{2}, \cos\theta/\sqrt{2}, \sin\theta)^{\mathrm{T}}$ and $\mathbf{q} = (1/\sqrt{2}, 1/\sqrt{2}, 0)^{\mathrm{T}}$. Consequently, the shear

modulus in the plane (x, x_3) is

$$\frac{c_s}{c_{11}} = \frac{c_{44}}{c_{11}} - \frac{1}{2}\zeta \cos^2\theta. \tag{33}$$

Fig. 4b plots function (33) in the polar coordinates, using the parameter ζ for Cu. The shear stiffness minimizes at $\theta = 0$ and π. Consequently, the shear modulus anisotropy favors the [0 0 1] stripes.

The [0 0 1] stripes induce a plane strain deformation in the plane (x_1, x_3). The $[\bar{1}\,1\,0]$ stripes induce a plane strain deformation in the plane (x_2, x_3). The deformation fields of two cases involve both the tensile and the shear moduli. For Cu (1 1 0) surface, the compliant directions in tension and in shear are different, so that one cannot select the stripe orientation from the elementary consideration of the stiffness. By contrast, one can confirm that the relevant shear modulus for the (1 0 0) substrate is isotropic. Consequently, if the surface stress slope is isotropic, stripes along the most compliant direction in tension will relax elastic energy the most for (1 0 0) surface, as shown by Lu and Suo (2002b).

Now consider the effect of the surface stress anisotropy. The elastic field in the substrate is linear in the slope tensor. Consequently, from Eq. (6), the free energy is quadratic in the slope tensor, and does not change if both ϕ_1 and ϕ_2 change sign simultaneously. We only need to consider ω in the range $-\pi/4 \leqslant \omega < 3\pi/4$, namely, in the upper right half-plane in Fig. 3. A more convenient anisotropy parameter is defined as

$$A = \sin\left(\omega - \frac{\pi}{4}\right) = \frac{\phi_2 - \phi_1}{\sqrt{2}\phi}, \tag{34}$$

which is in the range $-1 \leqslant A < 1$. Fig. 3 shows representative values of A in the plane (ϕ_1, ϕ_2). When $A = 0, \phi_1 = \phi_2$, and the slope tensor is isotropic. When $-1 < A < 0$, $|\phi_1| > |\phi_2|$, and the surface stress anisotropy favors the [0 0 1] stripes over the $[\bar{1}\,1\,0]$ stripes. When $0 < A < -1, |\phi_1| < |\phi_2|$, and the surface stress anisotropy favors the $[\bar{1}\,1\,0]$ stripes over the [0 0 1] stripes.

We then examine the combined effect of stiffness anisotropy and surface stress anisotropy. For the time being, the phase boundary energy is taken to be isotropic ($\gamma = 0$). Fig. 5 draws the function $\Psi(\theta)$ for Cu (1 1 0) surface. Depending on A, the function $\Psi(\theta)$ reaches minimum at different values of θ. We next discuss these results.

Of the three plots in Fig. 5, the easiest to interpret is Fig. 5b. When $A = 0$, the surface stress tensor is isotropic, so that the $\Psi(\theta)$ curve reflects the effect of stiffness anisotropy. The function $\Psi(\theta)$ reaches two local minima at $\theta = 0°$ (i.e., the [0 0 1] stripes), and at $\theta = 90°$ (i.e., the $[\bar{1}\,1\,0]$ stripes). The [0 0 1] stripes have lower free energy than the $[\bar{1}\,1\,0]$ stripes. That is, the orientation most compliant in shear prevails over that most compliant in tension. This conclusion appeals to the intuition as the surface stress nonuniformity induces a surface shear traction on the substrate. As A becomes positive, the surface stress anisotropy favors the $[\bar{1}\,1\,0]$ stripes over the [0 0 1] stripes, so that the minimum at $\theta = 0°$ goes up, and the minimum at $\theta = 90°$ goes down. Above a critical value, $A_c = 0.0323$, the minimum at $\theta = 0°$ is higher than that at $\theta = 90°$. That is, a tiny bias of $|\phi_2|$ over $|\phi_1|$ can override the stiffness anisotropy,

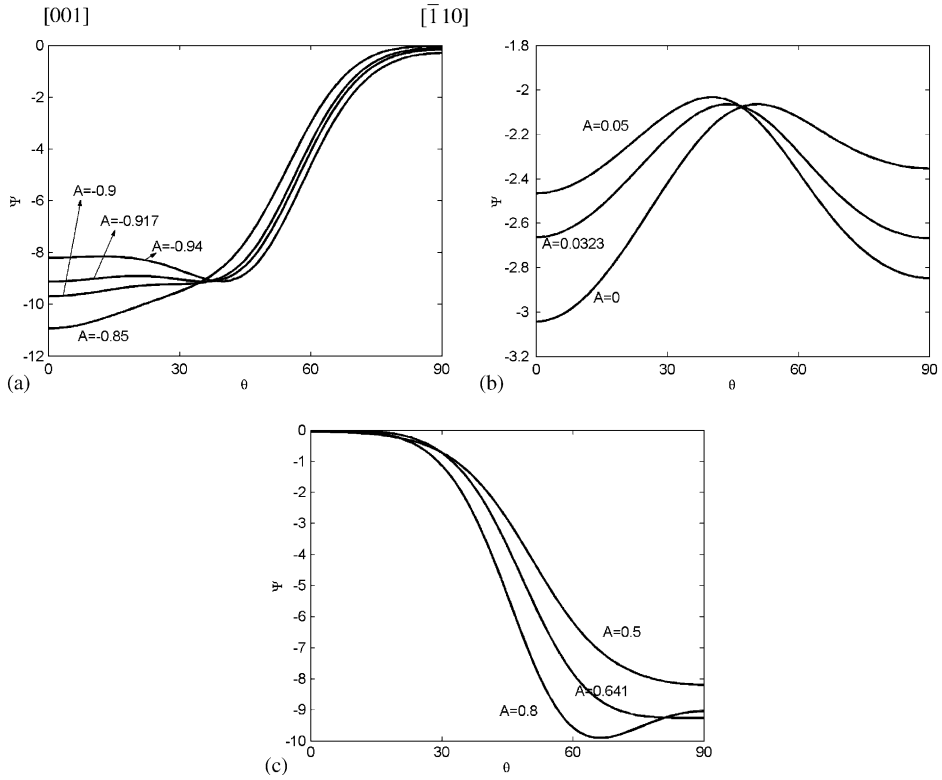

Fig. 5. Ψ as a function of the stripe orientation θ for Cu (1 1 0) surface, with various degrees of surface stress anisotropy, A: (a) near the [0 0 1]-to-θ transition, $A_c = -0.917$: (b) near the [0 0 1]-to-[$\bar{1}$ 1 0] transition, $A_c = 0.0323$; (c) near the [$\bar{1}$ 1 0]-to-θ transition, $A_c = 0.641$.

leading to the transition from the [0 0 1] stripes to the [$\bar{1}$ 1 0] stripes. The transition is of the first order.

Another transition occurs as A increases more (Fig. 5c). Above a critical value, $A_c = 0.641$, a new minimum appears at an orientation off the axis [$\bar{1}$ 1 0], while the free energy of the [$\bar{1}$ 1 0] stripes becomes a local maximum. The transition is of the second order. This kind of transition was first discovered for the case that the substrate has isotropic stiffness (Lu and Suo, 2002a; Gao et al., 2002). In that case, the transition occurs when ϕ_2 is significantly negative and ϕ_1 is positive. The transition on the Cu (1 1 0) surface is analogous, except that the stiffness anisotropy significantly enlarges the domain of the off-axis stripes, which can even occur when both ϕ_1 and ϕ_2 are of the same sign. When the stripes are off the crystalline axes, symmetry ensures that two variants of the stripes, making positive and negative angles ($\pm\theta$) from one principal axis, have the identical free energy. These two variants will form a herring-bone structure. We refer readers to Gao et al. (2002) for a physical interpretation of the along-axis to off-axis transition.

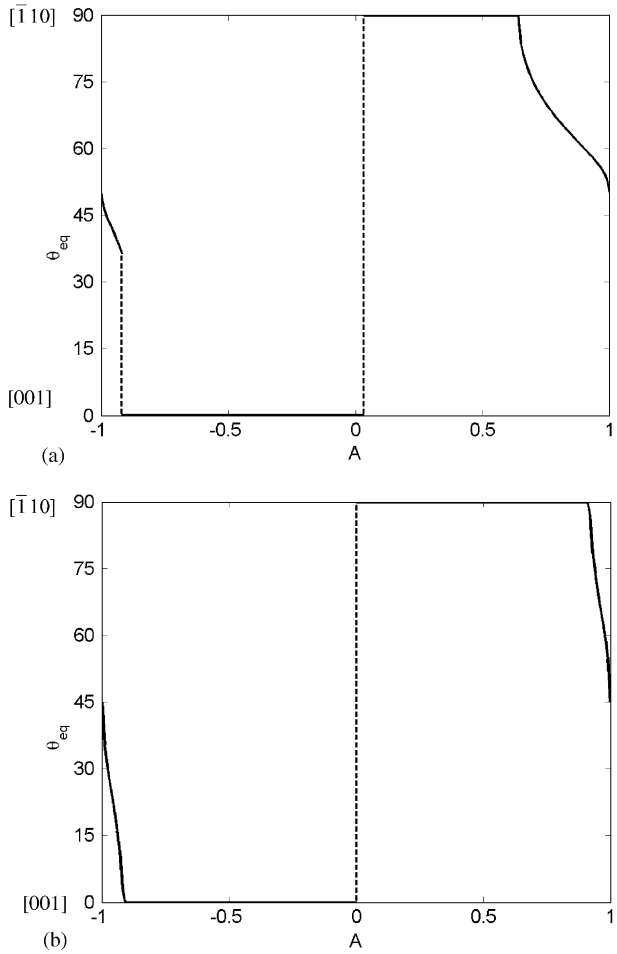

Fig. 6. The equilibrium orientation, θ_{eq}, as a function of A for Cu (1 1 0) surface; (b) the equilibrium orientation, θ_{eq}, as a function of A for elastically isotropic surface.

Finally, we look at negative A (Fig. 5a). Yet another transition occurs at a significantly negative value ($A_c = -0.917$). The [0 0 1] stripes transform to two variants of stripes at $\pm\theta$ orientations off the crystal axis. When $A > A_c$, the function $\Psi(\theta)$ reaches a global minimum at $\theta = 0°$. When A is somewhat large than A_c, a new local minimum appears at an angle $\theta > 0°$. Initially, this new minimum is higher than that at $\theta = 0°$. However, as A becomes more negative, below A_c, the new minimum becomes lower than that at $\theta = 0°$. Consequently, the transition is of the first order.

Fig. 6a shows the equilibrium orientation θ_{eq} as a function of the surface stress anisotropy A. The three transitions are evident. The first order transitions are denoted by the dashed lines, and the second order one by the solid line. For comparison, Fig. 6b shows the corresponding function for the case that the substrate is elastically isotropic,

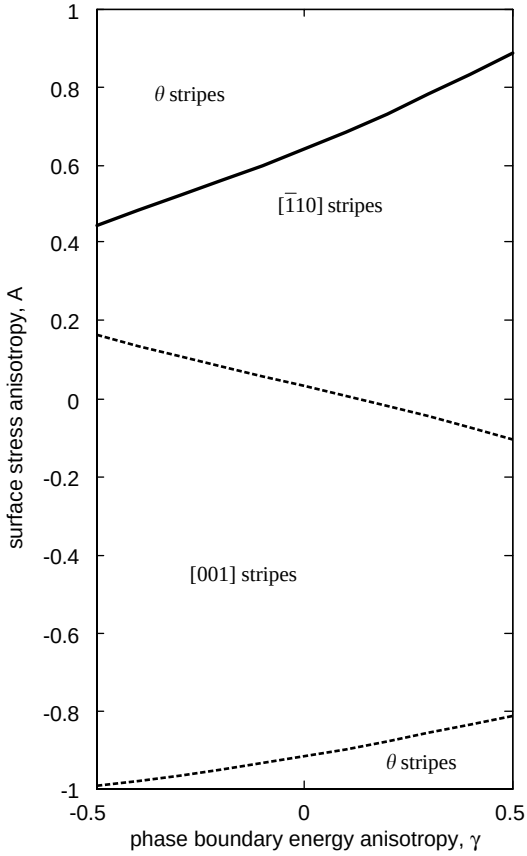

Fig. 7. Phase diagram with varying A and γ for Cu (1 1 0) surface.

with Poisson's ratio being 0.3. The elastic anisotropy in Cu slightly shifts the critical A for the [0 0 1]-to-[$\bar{1}$ 1 0] transition. The [$\bar{1}$ 1 0]-to-θ transition for Cu (1 1 0) happens at a value of A lower than that for an elastically isotropic substrate. The [0 0 1]-to-θ transition for Cu (1 1 0) happens at a value of A similar to that for an elastically isotropic substrate, the former being of the first order and the latter being of the second order.

The anisotropy of the phase boundary energy is measured by parameter γ. Varying both A and γ, we can construct a phase diagram for Cu (1 1 0) as shown in Fig. 7. When $\gamma = 0$, the transitions have already been shown in Fig. 6. As we stated before, a negative γ favors the [0 0 1] stripes over the [$\bar{1}$ 1 0] stripes, and the opposite is true for a positive γ. The trend is clearly recovered in the phase diagram. Because the free energy is invariant when both ϕ_1 and ϕ_2 change sign simultaneously, $A = 1$ and $A = -1$ are equivalent, and the two regions of θ stripes are connected.

The Cu (1 1 0)-(2 × 1)O system in the experiment of Kern et al. (1991) forms [0 0 1] stripes. At this time of writing, we lack the knowledge of the anisotropy of the surface

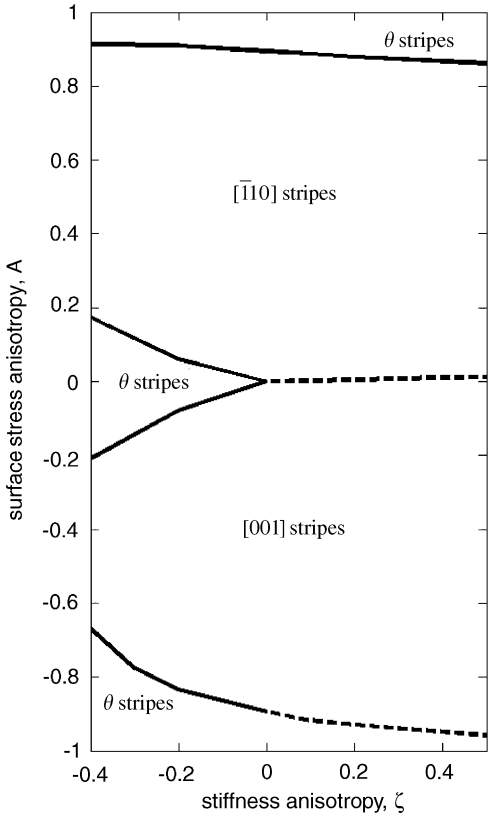

Fig. 8. Phase diagram with varying A and ζ for (1 1 0) surface of a cubic crystal.

stress tensor and phase boundary energy, and refrain from comparing our phase diagram with the experimental observations. We are unaware of any experimental observations of the $[\bar{1}\,1\,0]$ stripes or the θ stripes on (1 1 0) surface.

Finally, we explore the effect of stiffness anisotropy for other cubic crystals. Fig. 8 shows a phase diagram for the (1 1 0) surface of a cubic crystal, with $\eta = 0.5$ and $\gamma = 0$, and varying A and ζ (which measures the stiffness anisotropy of a cubic crystal). When $\zeta > 0$, similar to Cu (1 1 0), we see the transition from the θ stripes, to the [0 0 1] stripes, to the $[\bar{1}\,1\,0]$ stripes, and back to the θ stripes. When $\zeta < 0$, a new region of θ stripes appear. From this region, the transitions to the [0 0 1] stripes and to the $[\bar{1}\,1\,0]$ stripes are both of the second order.

6. Concluding remarks

The orientation of monolayer stripes depends on the anisotropy of the system. Three modes of anisotropy are studied in this paper: the surface stress, the substrate stiffness,

and the phase boundary energy. We have focused on the (1 1 0) surface of cubic crystals. Depending on the degrees of anisotropy, the equilibrium stripes can orient along either the [0 0 1] axis, or the [$\bar{1}$ 1 0] axis, or at an certain angle from a principal axis. Remarkably, the [0 0 1]-to-[$\bar{1}$ 1 0] transition is mainly determined by the surface stress anisotropy, with anisotropy in stiffness tensor and phase boundary energy contributing weakly. The transition from the along-axis to the off-axis stripes can be either first or second order. At this writing, the experimental observations of stripes on (1 1 0) surfaces are very limited. Furthermore, the anisotropy in surface stress and that in phase boundary energy have not been characterized fully for relevant systems. We eagerly await new experiments along these lines.

Throughout this paper, we have assumed periodic stripes, which are one-dimensional patterns. When the stripes are off the crystalline axes, symmetry requires that two variants exist on (1 1 0) surface, and four variants on (1 0 0) surfaces. When studying two-dimensional phase patterns, we must incorporate the additional structural order parameters. The thermodynamics and kinetics of translational or rotational order parameters can be modeled in the Ginzburg–Landau formalism (Gao and Suo, 2002). The structural variants can coexist and further reduce the free energy, similar to the martensite transformation. We will discuss the two-dimensional phase patterns with both compositional and structural order parameters in subsequent papers.

Acknowledgements

The work is supported by the Department of Energy through contract DE-FG02-99ER45787.

Appendix A. The anisotropic elasticity boundary value problem

The appendix solves the elastic field in a semi-infinite anisotropic space subject to arbitrary surface traction. This elastic field depends on three spatial coordinates, but is a superposition of many Fourier components, each being a plane field. We solve each plane field by using the Stroh (1958) method.

A combination of Eqs. (2), (3) and (10) gives the well-known equations that govern the elastic displacements

$$c_{ijkl}u_{k,lj} = 0. \tag{A.1}$$

We will first find the general solution to this set of partial differential equation, and then use the boundary conditions to determine the elastic field in the semi-infinite substrate.

Let (h_1, h_2) be a unit vector in the (x_1, x_2) plane. We look for solution of the form

$$u_l = A_l f(z), \quad z = h_1 x_1 + h_2 x_2 + p x_3. \tag{A.2}$$

Here f is a one-variable function, p a scalar, and A_l a vector. As will be clear shortly, p is a complex number. Eq. (A.2) represents a plane field in that the displacement vector depends on two spatial coordinates in the plane spanned by x_3 and the vector

(h_1, h_2). Representation like (A.2) has been used by Barnett and Lothe (1985) to study Rayleigh waves on the surface of anisotropic solids.

To see the algebraic structure, we write $p = h_3$. Substituting Eq. (A.2) into Eq. (A.1), we obtain that

$$c_{ijlm} h_j h_m A_l = 0. \tag{A.3}$$

This is a generalized eigenvalue problem, p being the eigenvalue and A_l the eigenvector. In the above, we have eliminated the factor $\mathrm{d}^2 f/\mathrm{d}z^2$. Once p and A_l satisfy Eq. (A.3), with any differentiable function $f(z)$, the displacement field (A.2) satisfies the partial differential equations (A.1). The problem of solving a set of partial differential equations now becomes one of solving an algebraic eigenvalue problem.

The characteristic equation

$$\det(c_{ijlm} h_m h_j) = 0, \tag{A.4}$$

is a sixth order polynomial in p with real coefficients. The roots of the polynomial are the eigenvalues. All eigenvalues must be complex; for if p were real, the matrix $c_{ijlm} h_m h_j$ would be positive-definite, and the linear equations (A.3) would have no solution. Consequently, the six roots form three pairs of complex-conjugate. Denote the three roots with positive imaginary parts by p_a, $a = 1, 2, 3$, and the corresponding eigenvectors by A_{ka}. Each eigenvector is determined up to a complex constant. Once the stiffness tensor c_{ijkl} is prescribed, for a given direction (h_1, h_2), one can solve this eigenvalue problem numerically.

We now have three complex variables, $z_a = h_1 x_1 + h_2 x_2 + p_a x_3$, $a = 1, 2, 3$. Let $f_1(z_1)$, $f_2(z_2)$, $f_3(z_3)$ be three arbitrary analytical functions. The displacement field is a linear superposition:

$$u_l = \sum_a A_{la} f_a(z_a) + \sum_a \bar{A}_{la} \bar{f}_a(\bar{z}_a). \tag{A.5}$$

A bar on the top of a quantity denotes the complex conjugate. This form ensures that the displacement is real-valued. Eq. (A.5) is the general solution to (A.1) for the displacement field that depends on two spatial coordinates in the plane spanned by x_3 and the vector (h_1, h_2).

The traction on the plane normal to the x_3 axis, $\mathbf{t} = (\sigma_{13}, \sigma_{23}, \sigma_{33})^{\mathrm{T}}$, is

$$\sigma_{i3} = \sum_a L_{ia} f'_a(z_a) + \sum_a \bar{L}_{ia} \bar{f}'_a(\bar{z}_a), \tag{A.6}$$

where the three vectors L_{ia} are defined as

$$L_{ia} = (c_{i3l1} h_1 + c_{i3l2} h_2 + c_{i3l3} p_a) A_{la}. \tag{A.7}$$

Stroh (1958) showed that the following matrix is a positive-definite Hermitian:

$$B = \mathrm{i} A L^{-1}. \tag{A.8}$$

When we fix an arbitrary scalar for each of eigenvector A_{la}, the same scalar affects L_{ia}. However, the matrix B is unaffected by the choice of the scalar, and has the same dimension as the compliance tensor. Split the matrix into the real and the imaginary parts,

$B = 1/c_{1111}(M + \mathrm{i}N)$, so that M is symmetric and positive-definite, N is antisymmetric, and both are dimensionless. These matrices are calculated numerically.

The three functions $f_1(z_1)$, $f_2(z_2)$, $f_3(z_3)$ have to be determined by the boundary conditions. Following Suo (1990), we solve the boundary value problem as follows. Let ζ be any complex variable of the form $\zeta = h_1 x_1 + h_2 x_2 + q x_3$, where q is an arbitrary complex number with a positive imaginary part. Use the vector notation, $\mathbf{f}(\zeta) = [f_1(\zeta), f_2(\zeta), f_3(\zeta)]^{\mathrm{T}}$. On the plane $x_3 = 0$, the four complex variables, z_1, z_2, z_3, ζ, all equal $h_1 x_1 + h_2 x_2$, so that the traction vector and the displacement vector are

$$\mathbf{t} = L\mathbf{f}'(h_\alpha x_\alpha) + \bar{L}\bar{\mathbf{f}}'(h_\alpha x_\alpha), \tag{A.9}$$

$$\mathbf{u} = A\mathbf{f}(h_\alpha x_\alpha) + \bar{A}\bar{\mathbf{f}}(h_\alpha x_\alpha). \tag{A.10}$$

The semi-infinite half-space occupies the lower half-space, and its surface coincides with the plane $x_3 = 0$. Assume that the surface is subject to an arbitrary traction field, which is represented by the Fourier transform:

$$\mathbf{t} = \int\int \mathbf{a}(\kappa_1, \kappa_2) \exp(\mathrm{i}\kappa_1 x_1 + \mathrm{i}\kappa_2 x_2)\, \mathrm{d}\kappa_1\, \mathrm{d}\kappa_2. \tag{A.11}$$

To ensure the traction vector is real-valued, we require that $\mathbf{a}(-\kappa_1, -\kappa_2) = \bar{\mathbf{a}}(\kappa_1, \kappa_2)$. By the principle of linear superposition, we only need to find the solution of one Fourier component:

$$\mathbf{t} = \mathbf{a} \exp(\mathrm{i}\kappa_1 x_1 + \mathrm{i}\kappa_2 x_2) + \bar{\mathbf{a}} \exp(-\mathrm{i}\kappa_1 x_1 - \mathrm{i}\kappa_2 x_2). \tag{A.12}$$

We now need to find analytic functions $\mathbf{f}(\zeta)$ that both satisfy the traction boundary conditions (A.12), and vanishes in the substrate far below the surface, namely, $\mathbf{f}(\zeta) \to 0$ as $x_3 \to -\infty$. Let the magnitude of the wavevector be $\kappa = \sqrt{\kappa_1^3 + \kappa_2^2}$, and $\kappa_\alpha = \kappa h_\alpha$. An inspection gives the solution

$$L\mathbf{f}'(\zeta) = \bar{\mathbf{a}} \exp(-\mathrm{i}\kappa\zeta). \tag{A.13}$$

The fact that q in $\zeta = h_1 x_1 + h_2 x_2 + q x_3$ has positive imaginary part ensures that $\mathbf{f}(\zeta) \to 0$ as $x_3 \to -\infty$. From Eq. (A.13), one can readily obtain $f_1(\zeta)$ $f_2(\zeta)$, $f_3(\zeta)$. One then replaces the variable to $f_1(z_1)$, $f_2(z_2)$, $f_3(z_3)$, and calculates the displacement field from Eq. (A.5) and the stress field from Eq. (A.6). In particular, the displacement on the substrate surface is

$$\mathbf{u} = \frac{\bar{B}\mathbf{a}}{\kappa} \exp(\mathrm{i}\kappa_1 x_1 + \mathrm{i}\kappa_2 x_2) + \frac{B\bar{\mathbf{a}}}{\kappa} \exp(-\mathrm{i}\kappa_1 x_1 - \mathrm{i}\kappa_2 x_2). \tag{A.14}$$

Consequently, the elastic energy stored in the substrate per period is given by

$$\frac{\kappa_1 \kappa_2}{(2\pi)^2} \int_{-\pi/\kappa_2}^{\pi/\kappa_2} \int_{-\pi/\kappa_1}^{\pi/\kappa_1} \frac{1}{2} \mathbf{t}^{\mathrm{T}} \cdot \mathbf{u}\, \mathrm{d}x_1\, \mathrm{d}x_2 = \frac{\mathbf{a}^{\mathrm{T}} M \bar{\mathbf{a}}}{\kappa}. \tag{A.15}$$

Now it is straightforward to calculate the quantity central to this paper. When the concentration is given by the Fourier series (13), the traction boundary conditions (11) become

$$\sigma_{31} = \mathrm{i}\phi_1 \cos\theta \sum_{n=-\infty}^{+\infty} \frac{2n\pi C_n}{\lambda} \exp\left(\frac{\mathrm{i}2n\pi x}{\lambda}\right),$$

$$\sigma_{32} = \mathrm{i}\phi_2 \sin\theta \sum_{n=-\infty}^{+\infty} \frac{2n\pi C_n}{\lambda} \exp\left(\frac{\mathrm{i}2n\pi x}{\lambda}\right),$$

$$\sigma_{33} = 0. \tag{A.16}$$

Considering only one real-valued component, that is, for a given pair of $\pm n$, we can identify that $\kappa = 2n\pi/\lambda$, and

$$\mathbf{a} = (\mathrm{i}\phi_1 \kappa C_n \cos\theta,\ \mathrm{i}\phi_2 \kappa C_n \sin\theta,\ 0)^{\mathrm{T}}. \tag{A.17}$$

The elastic energy can be obtained by combining Eqs. (A.15) and (A.17). The final result is given in the body of the text.

References

Alerhand, O.L., Vanderbilt, D., Meade, R.D., Joannopoulos, J.D., 1988. Spontaneous formation of stress domains on crystal surfaces. Phys. Rev. Lett. 61, 1973–1976.

Barnett, D.M., Lothe, J., 1985. Free surface (Rayleigh) waves in anisotropic elastic half-spaces: the surface impedance method. Proc. R. Soc. London A 402, 135–152.

Cahn, J.W., Hilliard, J.E., 1958. Free energy of a nonuniform system. 1. Interfacial free energy. J. Chem. Phys. 28, 258–267.

Ellmer, H., Repain, V., Rousset, S., Croset, B., Sotto, M., Zeppenfeld, P., 2001. Self-ordering in two dimensions: nitrogen adsorption on copper (1 0 0) followed by STM at elevated temperature. Surf. Sci. 476, 95–106.

Gao, Y.F., Suo, Z., 2002. Domain dynamics in a ferroelastic epilayer on a paraelastic substrate. J. Appl. Mech. 69, 419–424.

Gao, Y.F., Lu, W., Suo, Z., 2002. A mesophase transition in a binary monolayer on a solid surface. Acta Mater. 50, 2297–2308.

Ibach, H., 1997. The role of surface stress in reconstruction, epitaxial growth and stabilization of mesoscopic structures. Surf. Sci. Rep. 29, 195–263 (Erratum. Surf. Sci. Rep. 35, 71–73).

Kern, K., Niehus, H., Schatz, A., Zeppenfeld, P., Goerge, J., Comsa, G., 1991. Long-range spatial self-organization in the adsorbate-induced restructuring of surfaces: Cu{110}-(2 × 1)O. Phys. Rev. Lett. 67, 855–858.

Leibsle, F.M., Flipse, C.F.J., Robinson, A.W., 1993. Structure of the Cu{1 0 0}-c(2 × 2)N surface: a scanning-tunneling-microscopy study. Phys. Rev. B 47, 15 865–15 868.

Li, D., Diercks, V., Pearson, J., Jiang, J.S., Bader, S.D., 1999. Structural and magnetic studies of fcc Fe films with self-organized lateral modulation on striped Cu(1 1 0)-O(2 × 1) substrates. J. Appl. Phys. 85, 5285–5287.

Lu, W., Suo, Z., 1999. Coarsening, refining, and pattern emergence in binary epilayers. Z. Metallkd. 90, 956–960.

Lu, W., Suo, Z., 2001. Dynamics of nanoscale pattern formation of an epitaxial monolayer. J. Mech. Phys. Solids 49, 1937–1950.

Lu, W., Suo, Z., 2002a. Symmetry breaking in self-assembled monolayers on solid surface. I. Anisotropic surface stress. Phys. Rev. B 65, 085401.

Lu, W., Suo, Z., 2002b. Symmetry breaking in self-assembled monolayers on solid surfaces. II. Anisotropic substrate elasticity. Phys. Rev. B 65, 205418.

Ng, K.-O., Vanderbilt, D., 1995. Stability of periodic domain structures in a two-dimensional dipolar model. Phys. Rev. B 52, 2177–2183.

Plass, R., Last, J.A., Bartelt, N.C., Kellogg, G.L., 2001. Self-assembled domain patterns. Nature 412, 875–875.

Pohl, K., Bartelt, M.C., de la Figuera, J., Bartelt, N.C., Hrbek, J., Hwang, R.Q., 1999. Identifying the forces responsible for self-organization of nanostructures at crystal surfaces. Nature 397, 238–241.

Stroh, A.N., 1958. Dislocations and cracks in anisotropic elasticity. Philos. Mag. 7, 625–646.

Suo, Z., 1990. Singularities, interfaces and cracks in dissimilar anisotropic media. Proc. R. Soc. London A 427, 331–358.

Suo, Z., Lu, W., 2000. Composition modulation and nanophase separation in binary epilayer. J. Mech. Phys. Solids 48, 211–232.

Zeppenfeld, P., Krzyzowski, M.A., Romainczyk, Ch., Comsa, G., Lagally, M.G., 1994. Size relation for surface systems with long-range interactions. Phys. Rev. Lett. 72, 2737–2740.

Zeppenfeld, P., Krzyzowski, M.A., Romainczyk, Ch., David, R., Comsa, G., Röder, H., Bromann, K., Brune, H., Kern, K., 1995. Stability of disk and stripe patterns of nanostructures at surfaces. Surf. Sci. 342, L1131–L1136.